Eur. Phys. J. Special Topics **226**, 889–904 (2017)

DOI: 10.1140/epjst/e2016-60233-y

THE EUROPEAN PHYSICAL JOURNAL SPECIAL TOPICS

Regular Article

Study of the molecular mobility of (±)-methocarbamol in the amorphous solid state

Joaquim J. Moura Ramos[1], and Hermínio P. Diogo[2,a]

[1] CQFM – Centro de Química-Física Molecular and IN – Institute of Nanoscience and Nanotechnology, Instituto Superior Técnico, Universidade de Lisboa, 1049-001 Lisboa, Portugal

[2] CQE – Centro de Química Estrutural, Complexo I, Instituto Superior Técnico, Universidade de Lisboa, 1049-001 Lisboa, Portugal

Received 20 July 2016 / Received in final form 4 October 2016
Published online 18 April 2017

Abstract. The experimental techniques of differential scanning calorimetry (DSC) and thermally stimulated depolarization currents (TSDC) were used to study the thermal behavior of the pharmaceutical drug (±)-methocarbamol and its slow molecular mobility (in the 10^{-3}–10^{-2} Hz range) in the amorphous solid state. The possibility of polymorphism was considered based on the DSC results. The glass forming ability and the glass stability were investigated by DSC, and the general kinetic features of the main relaxation, including the fragility or steepness index, were studied by both experimental techniques. The secondary relaxations detected by TSDC revealed fast and slow (Johari-Goldstein) modes. These secondary relaxations of different nature were assigned based on physical aging studies.

1 Introduction

The molecular structure of most modern active pharmaceutical ingredients (APIs) is extremely complex, with the consequent low water-solubility of their crystalline form. On the other hand, the drugs in the higher energy amorphous solid state show a higher solubility and a faster dissolution rate, which leads to a higher bioavailability. Therefore it has the greatest interest to take advantage of this behavior for an effective formulation of poorly water-soluble drugs [1–3]. The use of drugs in the amorphous state has however the disadvantage of the glass instability (its tendency to crystallize), and this instability greatly varies from substance to substance, and depends also on the amorphization method (freeze drying, ball milling, melt quenching, cryo-milling) [4,5]. There seems no doubt that there is a close relationship between the physical instability of the amorphous and its molecular mobility [6,7]. The α-relaxation assists amorphous crystallization at temperatures below T_g [7–9], and a correlation was observed between the relaxation time of the Johari-Goldstein relaxation and the physical instability of the glass [6,10]. The local mobility also appears

[a] e-mail: hdiogo@tecnico.ulisboa.pt

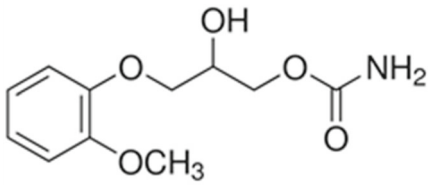

Fig. 1. The chemical structure of methocarbamol.

to have an important role at low temperatures, tens of degrees below T_g, where cooperative mobility and molecular diffusion are greatly reduced or nonexistent [11,12].

When the amorphous drug is unstable, stabilization of the glassy form is achieved by obtaining a glassy mixture of the API in a polymer matrix (the amorphous solid dispersion) [13,14] or through the so-called co-amorphous mixtures [15,16]. However, understanding the molecular mobility in pure APIs remains important and useful to find the best method of stabilization, and to design the most appropriate mixtures.

This work is a study by differential scanning calorimetry (DSC) and thermally stimulated depolarization currents (TSDC) of the slow molecular mobility in the amorphous solid state of (±)-methocarbamol, a muscle relaxant used to treat muscle pain and stiffness [17], that is a racemic mixture, i.e. a mixture of two enantiomers of the molecule depicted in Figure 1. It is a central nervous depressant with sedative and musculoskeletal relaxant properties that works by blocking nerve impulses (or pain sensations) that are sent to the brain. Methocarbamol is used together with rest and physical therapy to relieve the discomfort caused by acute (short-term) muscle or bone conditions such as pain or injury. It may also be used for other purposes. In our study we will use DSC first to characterize the thermal behavior: polymorphism, melting, crystallization, glass transition, glass forming ability, glass stability and tendency for crystallization on cooling from the equilibrium melt. Then we will use this technique to characterize the structural relaxation in amorphous methocarbamol. The TSDC results, on the other hand, will allow analyzing the different relaxations, including the cooperative and the local mobilities. The obtained results will be compared with those reported in the literature.

2 Experimental

2.1 Materials

(±)-Methocarbamol, empirical formula $C_{11}H_{15}NO_5$, CAS number: 532-03-6, molar weight $M_w = 241.24\,\mathrm{g\,mol^{-1}}$, was purchased from TCI (Lot ADHCA, purity > 99%) and was used without further purification. The melting temperature, taken as the endothermic peak's maximum, was found to be $T_{fus} = 96.7°\mathrm{C}$ (see dashed line in Fig. 3, red in the online edition), and the melting enthalpy was determined as $\Delta H_{fus} = 39.22\,\mathrm{kJ\,mol^{-1}}$, in reasonable agreement with the published values (see Tab. 1). The melting point of both the pure enantiomers is reported to be ∼110°C [17,18], with melting enthalpy $\Delta \mathrm{H}_{fus} = 42.80\,\mathrm{kJ\,mol^{-1}}$ [18]. The chemical structure of methocarbamol is shown in Figure 1.

2.2 Techniques

2.2.1 Differential Scanning Calorimetry (DSC)

The calorimetric measurements were performed with a 2920 MDSC system from TA Instruments Inc.. The samples of ∼5–10 mg were introduced in aluminium pans.

Table 1. Thermodynamic properties of methocarbamol determined in the present work, compared with values reported in the literature.

	This work	Literature
T_{fus}/°C	96.7	98.06[17]; 95.4[30]; 97.7[31]; 93.8[18,32]
ΔH_{fus} / kJ mol^{-1}*	39.22	39.54[17]; 38.6[30]; 40.06[31]; 37.45[18]
T_g/°C	2.0* (DSC); −3.8(TSDC)	3.25 (DSC)[30]; −2.1 (DRS**)[30]
ΔC_p (J K^{-1} g^{-1})	0.859 ± 0.035***	

* Onset on heating at 10°C/min.
** Dielectric relaxation spectroscopy (DRS).
*** Mean over 38 determinations using conventional DSC at different heating rates (from 2 to 15°C/min).

The measuring cell was continuously purged with high purity helium gas at 30 mL min^{-1}. An empty aluminium pan, identical to that used for the sample, was used as the reference. Details of the calibration procedures are given elsewhere [19].

2.2.2 Thermally Stimulated Depolarization Currents (TSDC)

Thermally Stimulated Depolarization Current experiments were carried out with a TSC/RMA spectrometer (TherMold, Stamford, CT, USA) covering the range from −150 °C to +400 °C. For TSDC measurements the sample (thickness of ∼0.5 mm) was placed between the disc-shaped electrodes (7 mm diameter) of a parallel plane capacitor and immersed in an atmosphere of high purity helium (1.1 bar). Methocarbamol in the amorphous solid state was prepared by heating up to 10 to 15°C above the melting temperature followed by fast cooling (20°C min^{-1}) down to temperatures well below T_g (−50°C for instance).

TSDC has a low equivalent frequency ($\sim 2 \times 10^{-3}$ Hz) so that it has a high resolution power and is sensitive to slow molecular motions (from ∼5 to 300 seconds). Furthermore, the partial polarization (PP) experimental procedure (see below) allows probing narrow regions of the TSDC spectrum, i.e. narrowly distributed motional modes. The fact that the relaxation time of the motional processes is temperature dependent, and becomes longer as temperature decreases, allows to make it exceedingly long (freezing process) compared with the timescale of the experiment. As will be seen next this is the very core of the TSDC technique, which relies on the possibility of producing stable electrets at low temperatures by cooling down to those temperatures in the presence of a polarizing electric field; a clear and concise explanation of the experimental procedures provided by the techniques of thermally stimulated currents is available [20] and may be useful for the reader unfamiliar with this technique. Two important parameters in a TSDC experiment are the polarisation temperature, T_P, at which the polarising electric field is turned on, and the temperature $T'_P < T_P$ at which the field is turned off (see Fig. 2). The difference $T_P - T'_P$ is the width of the polarization window of the experiment.

If it is wide, the retained polarization (and of course the current peak that is the result of a TSDC experiment) will correspond to a complex set of energy distributed motional modes. Oppositely, the PP experiment where the polarizing field is applied in a narrow temperature interval, allows probing more narrowly distributed relaxation modes. In the conceptual limit of a very narrow polarization window, the experimental depolarisation current peak is supposed to correspond to a single mode of relaxation [21]. In the present work and in most of our previous ones we use polarisation windows two degrees wide ($\Delta T = T_p - -T'_p = 2$°C).

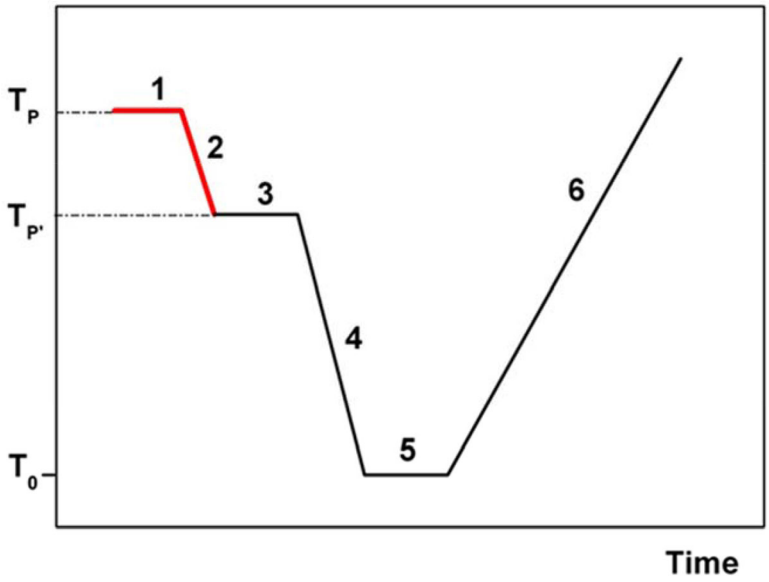

Fig. 2. Schematic diagram of the experimental procedure for a TSDC experiment. The width of the polarizing window is $\Delta T = T_P - T'_P$ and it is typically between 0 and 5 degrees in a narrow window partial polarization (PP) experiment. The electric field is on in steps 1 and 2 (thicker lines, red in the online version) and the depolarization current is recorded during the constant rate heating process (step 6).

The physical foundations of the TSDC experimental technique are presented in classical publications [22–24], while more recent review articles indicate various applications [25–29].

3 Results and discussion

3.1 General thermal behaviour

The curve of the DSC heat flow taken on cooling from the equilibrium melt did not show any crystallization signature for cooling rates between 2 and 20°C min^{-1}, indicating that methocarbamol has a strong glass forming ability. Furthermore, our DSC thermograms on heating from the amorphous solid state exhibited an exothermic signal of cold crystallization with an onset at ∼55°C and a maximum rate at ∼80°C followed by the endothermic melting peak (see continuous line in Fig. 3, blue in the online edition), confirming a previously reported observation [30]. Given that a glass is said to have a poor stability when it has an open path for crystallization, directly from the amorphous solid or by heating it above Tg (from the metastable liquid), the previous observations allow concluding that racemic methocarbamol displays weak glass stability. However, this instability did not prevent the study of the molecular mobility in the amorphous solid state, since the metastable liquid does not crystallize at temperatures below 40°C.

The insert of Figure 3 is part of the continuous line thermogram of the main figure and shows the signature of the glass transition (blue in the online edition). We reported before that the crystalline fresh, as received sample (crystal 1) melted at $T_{fus} = 96.7$°C; moreover, we verified that the thermogram (dotted line in Fig. 3, red in the on line edition) did not exhibit any exotherms, endotherms or signals other

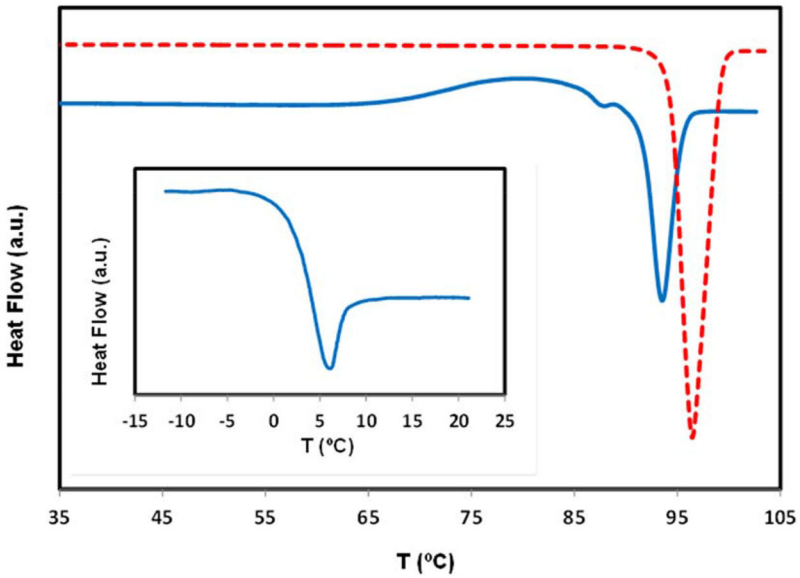

Fig. 3. DSC heat flow of methocarbamol obtained on heating (at $10\,^{\circ}\mathrm{C\,min^{-1}}$) the crystalline as received sample (dotted line) and the amorphous solid sample (continuous line). The insert shows the glass transition signal.

than that associated with the melt. On the other hand, the methocarbamol sample crystallized on heating from the metastable liquid (crystal 2) was obtained by heating the amorphous solid from $-50\,^{\circ}\mathrm{C}$ to $80\,^{\circ}\mathrm{C}$, at which temperature the rate of cold crystallization is high, and leaving an hour at this temperature to ensure complete crystallization. The sample was then cooled to $-50\,^{\circ}\mathrm{C}$ before being subjected to DSC fusion assays in the conventional and in the step by step modes. It was found that this crystalline sample (crystal 2) showed a melting temperature $T_{fus} = 93.4^{\circ}\mathrm{C}$, more than three degrees lower (see in Fig. 3 the melting peaks of the two presumed polymorphs), and a melting enthalpy $\Delta H_{fus} = 33.46\,\mathrm{kJ\,mol^{-1}}$, more than $5\,\mathrm{kJ\,mol^{-1}}$ lower than that of the as received sample (crystal 1). In order to test this possibility of the existence of two polymorphs of (±)-methocarbamol, we submitted the samples to an experimental protocol that causes the temperature to jump a specified number of degrees at a specified time interval until a final temperature, above the melting temperature, is reached. The experimental procedure, called *step by step scanning calorimetry*, is thus a heating process composed by successive isothermal steps, allowing a better insight on the kinetics of the melting process [33]. The two crystalline methocarbamol samples, the fresh as received one and that obtained by cold crystallization, were submitted to the step by step scanning procedure, and the results are presented in Figure 4, where the top line (red in the online edition) shows the experimental result (heat flow as a function of time), while the lower thinner line (blue in the online edition) schematically displays the experimental procedure (temperature as a function of time).

Note that, far from the melting temperature region, the heat flow in the different isothermal steps is nearly the same. In the melting temperature region of both samples, shown in Figure 4, one can identify two manifestations of the melting process: 1 – Melting on heating that occurs in the transition from one step to the next. This appears as an endothermic spike, given that increasing the heating rate leads to an amplification of the heat flow effects. 2 – Isothermal melting that occurs during the

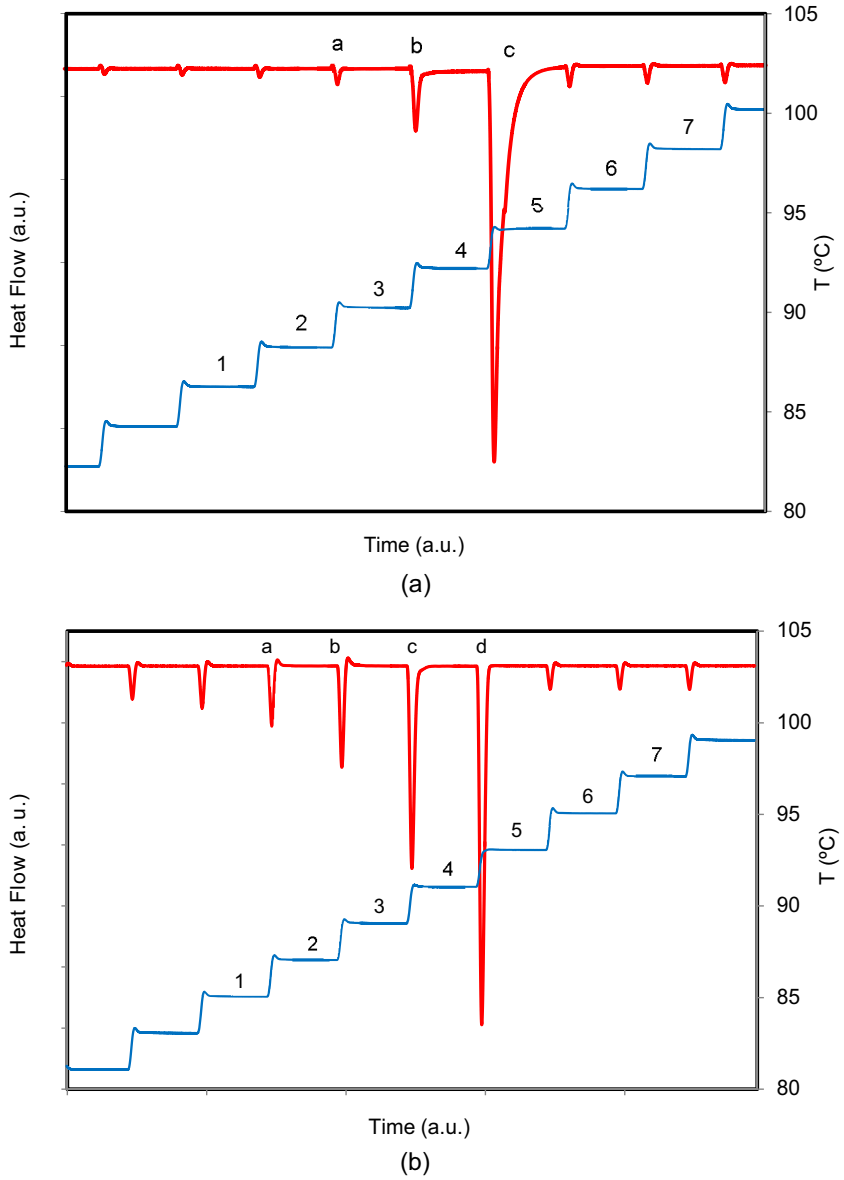

Fig. 4. Melting of (±)-methocarbamol obtained by step by step scanning calorimetry. The top curve shows the experimental result of the experiment (heat flow as a function of time, red in the online version), while the lower thinner line schematically displays the experimental procedure (temperature as a function of time, blue in the online version). The temperature jumps are $\Delta T = 2°C$, and the duration of the isothermal steps is $\Delta t = 10$ minutes. Figure (a) describes the behavior of the as received sample and the temperature at step 1 is 86°C while (b) corresponds to the sample formed by cold crystallization from the metastable liquid and the temperature at step 1 is 85°C.

isothermal steps, which is slow given the absence of the stimulating effect of the heating rate, and that only becomes apparent when large variations in the heat flow occur, as is the case in the isothermal 5 of Figure 4a.

Let us observe what happens when the melting temperature region is approached. Looking at Figure 4a, the appearance of the endothermic small peak "a" between steps 2 and 3 indicates the very beginning of the melting process, as the sample is heated up from 88 to 90°C. The strong endothermic peak "c" in the heat flow between steps 4 and 5 (as the sample is heated from 92 to 94°C) corresponds to the melting of most of the sample. Note that the melting process extends through the isothermal step 5 (at 94°C), in such a way that the heat flow decreases with increasing time, so that the melting is complete at the end of this isotherm since no thermal effect is observed at the next transition between the isotherms 5 and 6. From Figure 4a we can conclude that the as received sample melts in a "narrow" temperature interval between 90 and 94°C, the melting process being complete at the end of the isothermal at 94°C. On the other hand, from Figure 4b we see that the melting process of the sample obtained by cold crystallization (crystal 2) is slower, occurring in a wider temperature range. In fact, the endothermic small peak "a" that indicates the beginning of the melting process is now between steps 1 and 2, as the sample is heated up from 85 to 87°C (although an incipient melting may already be noted in the transition between the isotherms at 83 and 85°C). Furthermore, the strong endothermic peak "d" in the heat flow between steps 4 and 5 (as the sample is heated from 91 to 93°C) indicates the end of melting of the sample, this time not extending through the isothermal 5. From Figure 4b we can conclude that the sample obtained by cold crystallization melts in a wider temperature interval between 85 and 93°C.

We believe that the reported results on the melting process of the two samples, namely the different temperature locations and enthalpies of the DSC endothermic peak, as well as the different melting kinetics, allow us to conclude with reasonable certainty that we are in the presence of two polymorphs of racemic methocarbamol. Let us finally note that a third polymorph was also detected at $T_{fus} = 87.8\,^{\circ}\mathrm{C}$, but its appearance was unpredictable and in small quantities, so that it was not possible to understand the conditions for its formation.

3.2 Dynamic analysis of the glass transition by DSC

We are interested here in analyzing the influence of the heating rate on the temperature location of the glass transition signature, and we will consider two different ways of defining this location. The first, more conventional, is the extrapolated onset temperature (temperature at the intersection of the extrapolated baseline and the tangent taken at the point of maximum slope), T_{on}, and the second, recently suggested by Svodoba [34,35], is the temperature of the minimum heat flow (in the "exo up" configuration) at the endothermic overshoot, T_{ov}. We will calculate the activation energy of the structural relaxation, $E_a(T_g)$, from the heating rate, q^+, dependence of T_{on} and T_{ov}, using the relationship [36]:

$$\frac{d\left(\ln q\right)}{d\left(1/T_x\right)} = -\frac{E_a\left(T_g\right)}{R}, \tag{1}$$

where R is the gas constant and T_x is the temperature (T_{on} or T_{ov}) that defines the position of the DSC glass transition signal. The cooling/heating cycles were such that the ratio between the cooling and following heating rates, q^-/q^+, is unity. The results are plotted in Figure 5. The heating rate dependence of T_{ov} is shown as diamonds (blue in the online edition, left hand side of the figure, correlation coefficient $r^2 = 0.995$) and leads to an activation energy $E_a = 396\,\mathrm{kJ\ mol^{-1}}$.

The heating rate dependence of T_{on}, on the other hand, is shown as triangles (red in the online edition, right hand side of the figure, correlation coefficient $r^2 = 0.988$)

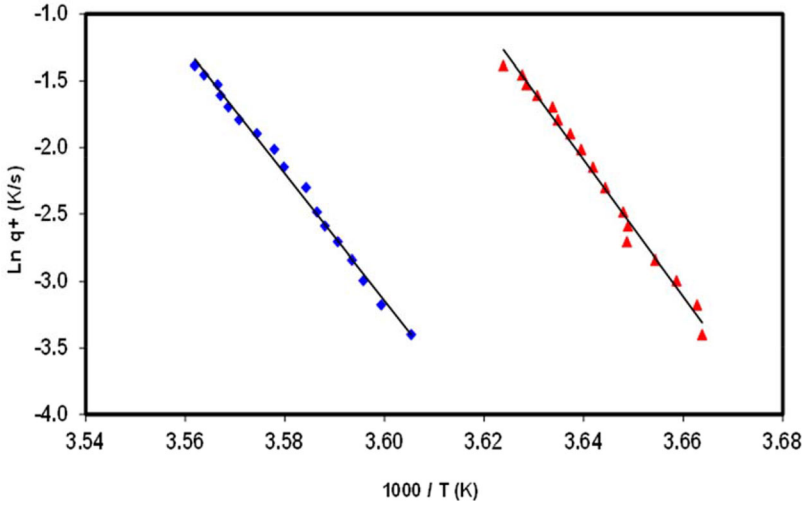

Fig. 5. "Arrhenius plots" of the logarithm of the heating rate, q^+, as a function of $1000/T_{ov}$ (diamonds, blue in the online edition) and of $1000/T_{on}$ (triangles, red in the online edition) where T_{ov} is the temperature of the overshoot peak and T_{on} is the temperature of the extrapolated onset of the glass transition signal. The experiments where designed in such a way that the ratio between the heating rate, q^+, and the previous cooling rate, q^- was unity: q^- / $q^+ = 1$.

and leads to an activation energy $E_a = 425$ kJ mol^{-1}. The fragility index, m, quantifies the steepness of the temperature dependence of the relaxation time close to T_g, and is defined as [37,38]:

$$m = \frac{E_a\,(T_g)}{2.303RT_g} \tag{2}$$

leading to $m_{DSC} = 75$ from T_{ov} and $m_{DSC} = 81$ from T_{on}.

The suspicion that the fragility (steepness index), a kinetic parameter, reflects somehow certain thermodynamic properties, led to the proposal of different forms to measure fragility based on thermodynamic quantities. One who had most success is described by the relationship

$$m = \frac{56.T_g.\Delta C_p\,(T_g)}{\Delta H_{fus}}, \tag{3}$$

with empirical origin [39,40], and which was later derived theoretically [41]. In (3) ΔC_p is the heat capacity jump at the glass transition temperature, and ΔH_{fus} is the melting enthalpy. The thermodynamic fragility calculated from equation (3) the thermodynamic quantities values in Table 1 is $m = 81$, in very good agreement with the value reported before, obtained from the heating rate influence on the temperature location of the DSC glass transition signature.

3.3 The molecular mobility studied by TSDC

In the following we will present the results of a series of narrow polarization window partial polarisation (PP) experiments performed on amorphous methocarbamol in the temperature region of the glass to metastable liquid transformation and below it. The result of each of those experiments is a current peak, $I(T)$, that is supposed

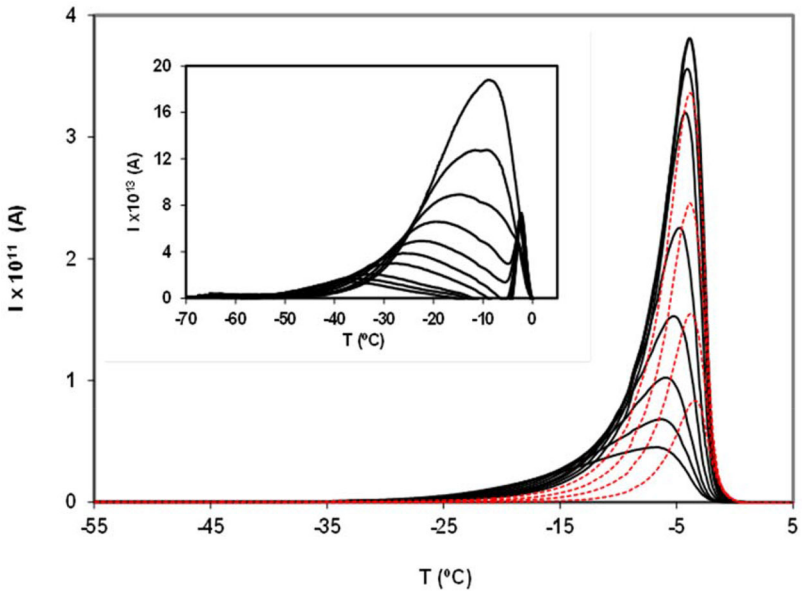

Fig. 6. Partial polarization (PP) peaks of the glass transition relaxation of methocarbamol obtained with a polarizing electric field strength of $E = 400\,\mathrm{V\ mm^{-1}}$ and polarization temperatures, T_p, from -20°C to 10°C in steps of 2 degrees, and from -10°C to -3°C in steps of 1 degree. The insert shows some PP peaks of a secondary mobility just below the glass transition relaxation, obtained with a polarizing electric field strength of $E = 350\,\mathrm{V\ mm^{-1}}$ and polarization temperatures, T_p, from -40°C to -20°C in steps of 2 degrees. In all the experiments the width of the polarization window was $\Delta T = 2^\circ$C, and the heating rate was $q = 4^\circ\mathrm{C\ min^{-1}}$.

to correspond to a narrow slice of mobility modes belonging to the wide continuous distribution that characterises the whole relaxation (see Sect. 1 of Ref. [20]).

3.3.1 The different relaxations and the relaxation map

Figure 6 shows a series of such current peaks in the temperature region of the glass to metastable liquid transformation that illustrate the features of the glass transformation as observed by TSDC. Let us first note that there is in the figure a partial polarization peak having maximum intensity (or area) higher than the other.

The temperature of maximum intensity, or temperature location, of this singular peak will be from now represented by T_M, while the temperature location of the other peaks will be represented generically by T_m. We find out from the figure that the PP peaks with maximum intensity at $T_m < T_M$ show increasing intensities, indicating that the polarizing field is allowed to polarize an higher number of cooperative motional modes as the polarization temperature, T_P, rises. On the other hand, the PP peaks with maximum intensity at $T_m > T_M$ (dashed lines, red in the online version) show decreasing intensities because the freezing-in of the polarization becomes more and more difficult as T_P increases through the glass to metastable liquid transformation region, indicating the rapid recovery of the non-equilibrium glass to the equilibrium state. The partial polarization peak with the largest maximum intensity (greater area, higher polarization) in the glass transition region, which is located at T_M, is the one where a higher extent of polarization was allowed to be "frozen-in," and it corresponds to a situation in which the electric field was allowed to polarize nearly all

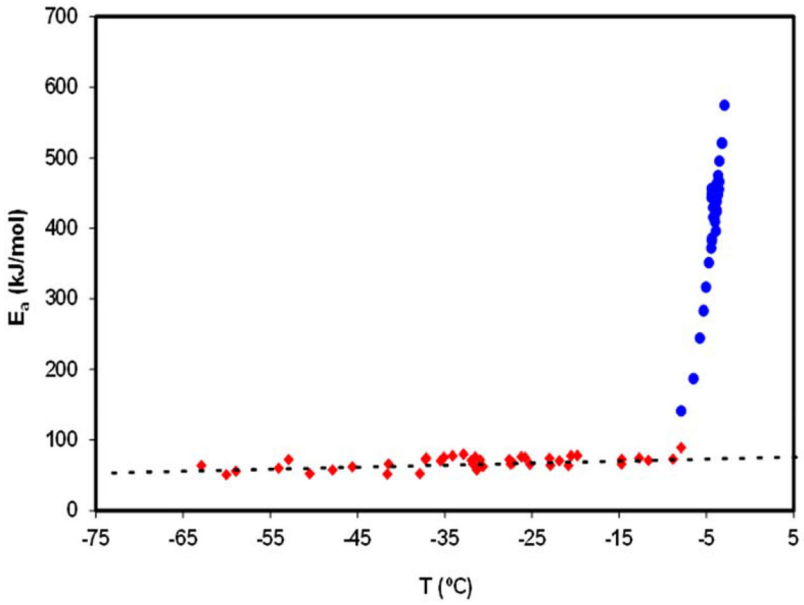

Fig. 7. Activation energy, $E_a(T_m)$, of the PP motional modes in the TSDC spectrum of methocarbamol as a function of the temperature of maximum intensity, T_m, of the corresponding current peak. The points above $\sim -8°$C (triangles, red in the online edition) refer to the motional modes of the alfa relaxation. The points below $\sim -8°$C (diamonds, blue in the online edition) correspond to modes of motion of the secondary relaxations (see text). The dashed line is the zero entropy line.

the higher activation energy motional modes associated with the glass transition relaxation. T_M thus represents a well-defined temperature in the glass transition range that can be considered as the glass transition temperature provided by the TSDC technique at the heating rate of the experiment. For the same reasons, the peak with maximum intensity at T_M was chosen for the determination of dynamic fragility of a glass forming substance from TSDC data [42–44] (see below).

The insert of Figure 6 shows some PP peaks taken in the temperature region near and below the glass to metastable liquid transformation. The sharp peak that is observed at $\sim -3°$C is a spontaneous discharge that is present in the baseline (scanning of the non-polarized sample), and therefore has no meaning in the context of the reorientational mobility. Apart from this detail, the peaks in this insert are the manifestation of a local mobility that persists in the glassy state and coalesce, at high temperatures, with the main relaxation modes.

The temperature dependent relaxation time, $\tau(T)$, associated to a given PP peak as those shown in Figure 6 is obtained by a standard treatment briefly explained in Section 2 of reference [20]. It contains all the kinetic information relative to the corresponding motional mode, so that the relevant kinetic parameters can be obtained by adjusting the $\tau(T)$ line to a suitable equation (Arrhenius, Vogel-Tammann-Fulcher [VTF], Williams-Landel-Ferry [WLF], ...). We will use the activation energy at the temperature of maximum intensity, $E_a(T_m)$, as a parameter to kinetically characterize each partial polarization mode. Figure 7 displays $E_a(T_m)$ of the motional modes (some of them in Fig. 6) as a function of T_m.

This representation is one among other forms of presenting the relaxation map of the studied system, where each point of coordinates $[T_m, E_a(T_m)]$ corresponds to a partial polarization peak, i.e. to a single or narrowly distributed mobility component.

The dotted line in Figure 7 is the so-called zero activation entropy line that depicts the behavior of the mobility modes with Arrhenius pre-factors close to the Debye value $\tau_0 \cong 10^{-13}$ s, typical of the local and non-cooperative thermally activated processes [45–48]; mobility with these characteristics corresponds to what is currently called secondary relaxations (see also Sect. 3 of Ref. [20]). The departure of $E_a(T_m)$ from the zero entropy line is an important kinetic feature of each motional mode. Let us note that −150°C is the lower limit of the temperature range accessible to the common TSDC equipment (liquid nitrogen as the cold source); since the value of the activation energy at this temperature in the zero entropy line is $E_a = 32$ kJ mol^{-1}, most TSDC apparatus just can detect local motions with activation energies higher than the mentioned value.

3.3.2 The α-relaxation and the dynamic fragility

The points at higher temperatures in Figure 7 (circles, blue in the online edition), correspond to PP peaks taken in the glass transition region (see main Fig. 6), and the activation energy of the corresponding motional modes strongly increases, away from the zero entropy line, as the temperature increases (from the amorphous solid to the metastable liquid state). The departure from the zero entropy line corresponds to an increase of the activation entropy, which is equivalent to a decrease of the Arrhenius pre-factor from its Debye value ($\tau_0 \cong 10^{-13}$ s). The amplitude of this departure is proportional to the dynamic fragility of the glass forming substance and is the manifestation of the cooperativeness of the molecular motions of the glass transition relaxation. In the framework of TSDC, the $\tau(T)$ line to be chosen to estimate the dynamic fragility is that which corresponds to the partial polarization peak with higher intensity in the glass transition region, located at $T_M \equiv T_g$, which leads to [44]:

$$m = \frac{E_a\,(T_M)}{2.303R.T_M} = \frac{T_M}{2.303R.\tau\,(T_M)}. \tag{4}$$

Since the dynamic fragility is proportional to the amplitude of the departure from the zero entropy line, we can alternatively calculate m from the coordinates of the point in Figure 7 that shows a greater departure from that line. From the TSDC data we estimated $m_{TSDC} = 108$ in reasonable agreement with the value $m = 129$ calculated from the parameters of the Vogel equation reported in a study by dielectric relaxation spectroscopy [30].

3.3.3 The secondary relaxations and aging

The points at lower temperatures in Figure 7, from ∼−8°C down to ∼−65°C (diamonds, red in the online edition), correspond to PP peaks taken below the glass transition region. They obey to the zero entropy line, i.e. they refer to mobility modes of the secondary relaxations. It is known that physical aging causes a loss of the cooperative mobility in the amorphous solid, which is at the origin of a decrease in the intensity of the TSDC depolarization peaks of the main relaxation. With regard to the secondary relaxations, it is customary to consider two types of different natures: the fast ones, with intramolecular nature (β-, γ-, δ-relaxations) and the slow one, with intermolecular nature (slow β or Johari-Goldstein (JG) relaxation). Those relaxations are detected in TSDC below the glass transition temperature, both behave according to the zero entropy line, and there is experimental evidence suggesting that they respond differently to physical aging [49–52]. The nature of the secondary relaxations

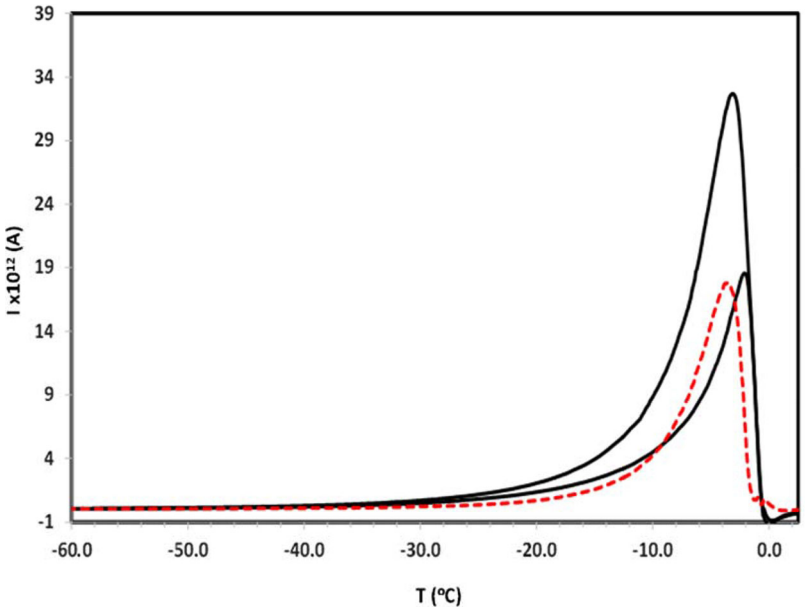

Fig. 8. Effect of aging on motional modes of methocarbamol probed by a wide polarization window experiment with polarization temperature $T_p = -10°C$ and a freezing temperature $T'_p = -100°C$, with a polarizing electric field of strength $E_p = 400$ V/mm. The higher intensity peak is the result of the experiment conducted with the fresh (non-aged) sample, while the other continuous peak refers to the sample aged at $T_{ag} = T_p = -10°C$ for $t_{ag} = 30$ min. The dashed curve (red in the online edition) is the difference between the two continuous peaks and corresponds thus to the mobility lost as a result of physical aging.

observed by TSDC in methocarbamol was thus analysed by looking at the influence of physical aging on the corresponding mobility modes, and Figure 8 displays relevant results on this subject. The experiments had wide polarization windows between a polarization temperature $T_p = -10°C$ and a freezing temperature $T'_p = -100°C$ (see Fig. 2), allowing exciting a large variety of secondary mobility modes and also some few low temperature cooperative modes of the main relaxation. Figure 8 shows two peaks drawn with a solid line: the highest intensity one is the result of an experiment conducted on the fresh, non-aged sample, while that with lower intensity was obtained performing the same experiment after aging the sample.

It is clear that the two continuous curves overlap for temperatures below $-35°C$, indicating that the lower temperature (fast) secondary motional modes (see Fig. 7) are not aging dependent. Rather, the mobility appearing in TSDC in the range between ~ -8 and $\sim -35°C$, which follows the zero entropy line (see Fig. 7), is sensitive to physical aging. The dashed line in Figure 8 (red in the online edition) was obtained by subtracting the continuous line curves, and represents the mobility lost as a result of aging. It confirms the previously reported observations: the dashed curve values are negligible (very close to zero) below $-35°C$ indicating that the corresponding mobility was not affected by aging; on the contrary, the secondary mobility appearing in the temperature range between ~ -35 and $\sim -8°C$ suffer a strong loss of mobility due to physical aging. We suggest therefore that the latter is a β_{JG} relaxation. There is experimental evidence showing that β_{JG}, detected by dielectric relaxation spectroscopy above T_g, persists in the glassy state, and that the temperature dependence of the relaxation time τ_{JG} above T_g is much stronger than below T_g [53,54]. This mobility, we believe to have a Johari-Goldstein nature, is detected by TSDC in

the glassy state (below T_g) and has an activation energy E_{aJG} distributed between ~64 and ~71 kJ mol^{-1} (see Fig. 7), which is characteristic of local movements which exist in amorphous solid. The Coupling Model [55] allows predicting the activation energy of the JG-relaxation, E_{aJG}, as [56];

$$E_{aJG}/RT_g = 2.303[2.8 - 13.7(1 - \beta_{KWW}) + \log_{10} f_\infty], \quad (5)$$

where β_{KWW} is the exponent of the Kohlrausch-Williams-Watts decay function and f_∞ is the pre-exponential factor of the Arrhenius equation written in terms of frequency. Taking $\beta_{KWW} = 0.49$ [30] and $\log_{10} f_\infty = 14.7$ reported for the non-JG secondary relaxations in methocarbamol [30], we calculated $E_{aJG} = 55$ kJ mol^{-1}. Despite the fact that this value has been calculated based on the prefactor of the non-JG secondary relaxation, it is not far from the energy interval reported before. Let us say also that the value 14.7, introduced in the calculation from equation (5), is in fact a lower limit of $\log_{10} f_\infty$ for JG (also known as slow β-relaxation) given that, unlike the local secondary mobility, the JG-relaxation has an intermolecular nature. A more precise calculation, starting from a value of $\log_{10} f_\infty > 14.7$ easily lead to a E_{aJG} value in the range mentioned above. In conclusion from what has been argued, we can say that the secondary relaxation observed by TSDC in (±)-methocarbamol, in the temperature range between −35 and −8°C and obeying the zero entropy line, corresponds to the β_{JG} process seen at $T < T_g$. The TSDC technique thus appears as useful for the analysis of the T-dependence of τ_{JG} in the glassy state.

Finally, the lower temperature mobility, which is displayed at $-65°C < T < -35°C$ in Figure 7, has activation energy, $E_{a\beta}$, distributed between ~55 and ~64 kJ mol^{-1}, Arrhenius pre-factor $f_0 = 1.6 \times 10^{12}$ Hz (the Debye frequency), and should correspond to the fast β-relaxation. These values seem reasonable given that: 1 – the activation energies are lower than those of the JG mobility; 2 – the pre-exponential factors, relaxation time or frequency, are the Debye values corresponding to zero activation entropy, typical of a non-cooperative local mobility. The kinetic parameters of this relaxation reported in the literature and obtained by DRS [30] are however significantly different: $E_{a\beta} = 40$ kJ mol^{-1} and Arrhenius pre-factor $f_0 = 10^{15}$ Hz. This discrepancy is observed frequently when comparing TSDC and DRS results for the fast β-relaxations, and was analysed before [48,50]. It arises from the fact that DRS provides the variation with temperature of the mean frequency (or relaxation time) of a continuous distribution, while TSDC provides the kinetic parameters of the elementary components of the continuous distribution.

4 Conclusions

The thermal behavior of methocarbamol, particularly its crystallization tendency on heating from the amorphous solid as well as on cooling from the equilibrium liquid, was investigated by differential scanning calorimetry. It was found that it has a strong glass forming ability and a week glass stability. The calorimetric results seem to indicate the existence of at least two polymorphs of racemic methocarbamol, which differ in their temperatures, enthalpies and kinetics of melting. The slow molecular mobility in amorphous methocarbamol was studied by differential scanning calorimetry and by thermally stimulated depolarization currents, allowing the determination of the kinetic parameters of the different relaxations. The activation energy of the structural relaxation was estimated from the heating rate dependence of the temperature location of the DSC glass transition signal, leading to a fragility index $m_{DSC} = 81$, in good agreement with the value calculated for the thermodynamic fragility. The TSDC analysis of the α-relaxation led to a dynamic fragility $m_{TSDC} = 108$ that

points to a fragile behavior of methocarbamol. The secondary relaxations appeared in TSDC in a wide temperature interval below T_g, between −65 and −8°C, and the aging analysis suggests the existence of two mobilities, different in nature. At the higher temperatures, preceding the α-relaxation, appears the Johari–Goldstein relaxation, with an activation energy $E_{aJG} = \sim 68\,\mathrm{kJ\ mol^{-1}}$. At lower temperatures the fast β-relaxation shows an activation energy $E_{a\beta} = \sim 60\,\mathrm{kJ\,mol^{-1}}$ and a Debye Arrhenius prefactor.

This work was partially supported by Fundação para a Ciência e a Tecnologia (FCT), Portugal (Projects UID/NAN/50024/2013 and UID/QUI/00100/2013) and COST Action CM1402 (from molecules to crystals – how do organic molecules from crystals).

References

1. B.C. Hancock, G. Zografi, Characteristics and significance of the amorphous state in pharmaceutical systems, J. Pharm. Sci. **86**, 1 (1997)
2. L. Yu, Amorphous pharmaceutical solids: preparation, characterization and stabilization, Adv. Drug. Delivery Rev. **48**, 27 (2001)
3. A.M. Kaushal, P. Gupta, A.K. Bansal, Amorphous drug delivery systems: molecular aspects, design, and performance, Crit. Rev. Ther. Drug. Carrier Syst. **21**, 133 (2004)
4. P. Karmwar, K. Graeser, K.C. Gordon, C.J. Strachan, T. Rades, Investigation of properties and recrystallisation behaviour of amorphous indomethacin samples prepared by different methods, Int. J. Pharm. **417**, 94 (2011)
5. A.W. Lim, K. Löbmann, H. Grohganz, T. Rades, N. Chieng, Investigation of physical properties and stability of indomethacin-cimetidine and naproxen-cimetidine co-amorphous systems prepared by quench cooling, coprecipitation and ball milling, J. Pharm. Pharmacol. **68**, 36 (2016)
6. S. Bhattacharya, R. Suryanarayanan, Local mobility in amorphous pharmaceuticals-characterization and implications on stability, J. Pharm. Sci. **98**, 2935 (2009)
7. K. Kothari, V. Ragoonanan, R. Suryanarayanan, Influence of molecular mobility on the physical stability of amorphous pharmaceuticals in the supercooled and glassy states, Mol. Pharm. **11**, 3048 (2014)
8. Y. Aso, S. Yoshioka, S. Kojima, Explanation of the crystallization rate of amorphous nifedipine and phenobarbital from their molecular mobility as measured by 13C nuclear magnetic resonance relaxation time and the relaxation time obtained from the heating rate dependence of the glass transition temperature, J. Pharm. Sci. **90**, 798 (2001)
9. S.P. Bhardwaj, K.K. Arora, E. Kwong, A. Templeton, S.D. Clas, R. Suryanarayanan, Correlation between molecular mobility and physical stability of amorphous itraconazole, Mol. Pharm. **10**, 694 (2013)
10. M. Mehta, V. Ragoonanan, G.B. McKenna, R. Suryanarayanan, Correlation between Molecular Mobility and Physical Stability in Pharmaceutical Glasses, Mol. Pharm. **13**, 1267 (2016)
11. M. Yoshioka, B.C. Hancock, G. Zografi, Crystallization of Indomethacin from the Amorphous State Below and Above Its Glass-Transition Temperature, J. Pharm. Sci. **83**, 1700 (1994)
12. K. Grzybowska, M. Paluch, A. Grzybowski, Z. Wojnarowska, L. Hawelek, K. Kolodziejczyk, K.L. Ngai, Molecular Dynamics and Physical Stability of Amorphous Anti-Inflammatory Drug: Celecoxib, J. Phys. Chem. B. **114**, 12792 (2010)
13. G. Van den Mooter, The use of amorphous solid dispersions: A formulation strategy to overcome poor solubility and dissolution rate, Drug. Discovery Today: Technologies **9**, e79 (2012)
14. T. Vasconcelos, S. Marques, J. das Neves, B. Sarmento, Amorphous solid dispersions: Rational selection of a manufacturing process, Adv. Drug. Delivery Rev. **100**, 85 (2016)

15. M.K. Riekes, A. Engelen, B. Appeltans, P. Rombaut, H.K. Stulzer, G. Van den Mooter, New Perspectives for Fixed Dose Combinations of Poorly Water-Soluble Compounds: a Case Study with Ezetimibe and Lovastatin, Pharm Res **33**, 1259 (2016)
16. S.J. Dengale, H. Grohganz, T. Rades, K. Löbmann, Recent advances in co-amorphous drug formulations, Adv. Drug. Delivery Rev. **100**, 116 (2016)
17. S. Alessi-Severini, F. Jamali, R.T. Coutts, F.M. Pasutto, *Methocarbamol* (Academic Press, San Diego, 1994), pp. 371–399
18. A.A. Bredikhin, Z.A. Bredikhina, D.V. Zakharychev, A.V. Pashagin, Chiral drugs related to guaifenesin: synthesis and phase properties of methocarbamol and mephenoxalone, Tetrahedron: Asymmetry **18**, 1239 (2007)
19. J.J. Moura Ramos, R. Taveira-Marques, H.P. Diogo, Estimation of the fragility index of indomethacin by DSC using the heating and cooling rate dependency of the glass transition, J. Pharm. Sci. **93**, 1503 (2004)
20. H.P. Diogo, M.T. Viciosa, J.J. Moura Ramos, Thermally Stimulated Currents: principles, methods for data processing and significance of the information provided, Supplementary Data to Thermochimica Acta **623**, 29 (2016)
21. G. Teyssedre, C. Lacabanne, Some considerations about the analysis of thermostimulated depolarization peaks, J. Phys. D: Appl. Phys. **28**, 1478 (1995)
22. J. van Turnhout, *Thermally Stimulated Discharge of Polymer Electrets* (Elsevier Sci. Pub. Co., Amsterdam, 1975)
23. R. Chen, Y. Kirsh, *Analysis of Thermally Stimulated Processes* (Pergamon Press, Oxford, 1981)
24. J. van Turnhout, *Thermally stimulated discharge of electrets*, in G.M. Sessler, editor. *Electrets* (Springer, Berlin, Heidelberg, 1987), pp. 81–215
25. V.M. Gun'ko, V.I. Zarko, E.V. Goncharuk, L.S. Andriyko, V.V. Turov, Y.M. Nychiporuk, R. Leboda, Skubiszewska-J. Zieba, A.L. Gabchak, V.D. Osovskii, Y.G. Ptushinskii, G.R. Yurchenko, O.A. Mishchuk, P.P. Gorbik, P. Pissis, J.P. Blitz, TSDC spectroscopy of relaxational and interfacial phenomena, Adv. Colloid. Interface Sci. **131**, 1 (2007)
26. B.B. Sauer, *Thermally Stimulated Currents: recent developments in characterisation and analysis of polymers*, in *Applications to Polymers and Plastics*, edited by S.Z.D. Cheng (Elsevier, Amsterdam, 2002), pp. 653–711
27. A. Vassilikou-Dova, I.M. Kalogeras, Dielectric analysis (DEA), in *Thermal Analysis of Polymers: Fundamentals and Applications*, edited by J.D. Menczel, R.B. Prime, 1st edn (John Wiley, Hoboken, New Jersey, 2009), pp. 497–613.
28. N. Boutonnet-Fagegaltier, A. Lamure, J. Menegotto, C. Lacabanne, A. Caron, H. Duplaa, M. Bauer, The use of thermally stimulated current spectroscopy in the pharmaceutical sciences, in *Thermal Analysis of Pharmaceuticals*, edited by D.Q.M. Craig, M. Reading (CRC Press, Boca Raton, 2007), pp. 359–382
29. S. Baker, M.D. Antonijevic, Thermal analysis - dielectric techniques, in *Solid State Characterization of Pharmaceutics*, edited by R.A. Storey, I. Ymén (Wiley, Chichester, UK, 2011), pp. 187–206
30. M.K. Saini, S.S.N. Murthy, Study of glass transition phenomena in the supercooled liquid phase of methocarbamol, acetaminophen and mephenesin, Thermochim Acta **575**, 195 (2014)
31. K.C. Mercado, G.A. Rodríguez, D.R. Delgado, F.Martínez, A. Romdhani, Solution thermodynamics of methocarbamol in some ethanol + water mixtures, Quím. Nova **35**, 1967 (2012)
32. A.A. Bredikhin, A.T. Gubaidullin, Z.A. Bredikhina, D.B. Krivolapov, A.V. Pashagin, I.A. Litvinov, Absolute configuration and crystal packing for three chiral drugs prone to spontaneous resolution: Guaifenesin, methocarbamol and mephenesin, J. Molec. Struct. **920**, 377 (2009)
33. J.J. Moura Ramos, H.P. Diogo, M.H. Godinho, C. Cruz, K. Merkel, Anomalous thermal behavior of salicylsalicylic acid and evidence for a monotropic transition to a nematic phase, J. Phys. Chem. B **108**, 7955 (2004)

34. R. Svoboda, J. Málek Description of enthalpy relaxation dynamics in terms of TNM model, J. Non-Cryst Solids **378**, 186 (2013)
35. R. Svoboda, How to determine activation energy of glass transition, J. Therm. Anal. Calorim. **118**, 1721 (2014)
36. C.T. Moynihan, A.J. Easteal, J. Wilder, J. Tucker, Dependence of the glass transition temperature on heating and cooling rate, J. Phys. Chem. **78**, 2673 (1974)
37. C.A. Angell, Relaxation in liquids, polymers and plastic crystals – strong/fragile patterns and problems, J. Non-Cryst. Solids **131–133**, 13 (1991)
38. R. Böhmer, C.A. Angell, Local and global relaxations in glass-forming materials, in *Disorder Effects on Relaxational Processes*, edited by R. Richert, A. Blumen (Springer-Verlag, Berlin, 1994), pp. 11–54
39. L.M. Wang, C.A. Angell, Response to Comment on Direct determination of the fragility indices of glassforming liquids by differential scanning calorimetry: Kinetic versus thermodynamic fragilities, J. Chem. Phys. **118**, 10351 (2003)
40. L.M. Wang, C.A. Angell, R. Richert, Fragility and thermodynamics in nonpolymeric glass-forming liquids, J. Chem. Phys. **125**, 074505 (2006)
41. X. Xia, P.G. Wolynes, Fragilities of liquids predicted from the random first order transition theory of glasses, Proc. Natl. Acad. Sci. USA **97**, 2990 (2000)
42. N.T. Correia, C. Alvarez, J.J. Moura Ramos, Fragility in side-chain liquid crystalline polymers: the TSDC contribution, Polymer **41**, 8625 (2000)
43. N.T. Correia, C. Alvarez, J.J. Moura Ramos, M. Descamps, Molecular motions in molecular glasses as studied by thermally stimulated depolarisation currents (TSDC), Chem. Phys. **252**, 151 (2000)
44. J.J. Moura Ramos, N.T. Correia, The Deborah number, relaxation phenomena and thermally stimulated currents, Phys. Chem. Chem. Phys. **3**, 5575 (2001)
45. H.W. Starkweather, Simple and complex relaxations, Macromolecules **14**, 1277 (1981)
46. H.W. Starkweather, Noncooperative relaxations, Macromolecules **21**, 1798 (1988)
47. H.W. Starkweather, Aspects of simple, non-cooperative relaxations, Polymer **32**, 2443 (1991)
48. N.T. Correia, JJ. Moura Ramos, On the cooperativity of the β-relaxation: A discussion based on dielectric relaxation and thermally stimulated depolarisation currents data, Phys. Chem. Chem. Phys. **2**, 5712 (2000)
49. J.J. Moura Ramos, H.P. Diogo, S.S. Pinto Local motions in L-iditol glass: identifying different types of secondary relaxations, Thermochim. Acta **467**, 107 (2008)
50. S.S. Pinto, J.J. Moura Ramos, H.P. Diogo, The slow molecular mobility in poly(vinyl acetate) revisited: new contributions from Thermally Stimulated Currents, Eur. Polym. J. **45**, 2644 (2009)
51. E. Mora, H.P. Diogo, J.J. Moura Ramos, The slow molecular dynamics in amorphous probucol, Thermochim. Acta **595**, 83 (2014)
52. H.P. Diogo, J.J. Moura Ramos, Contribution of the technique of thermostimulated currents for the elucidation of the nature of the Johari-Goldstein and other secondary relaxations in the vitreous state, IEEE Trans. Dielect. Elect. Insul. **21**, 2301 (2014)
53. M. Paluch, C.M. Roland, S. Pawlus, J. Ziolo, K.L. Ngai, Does the Arrhenius temperature dependence of the Johari-Goldstein relaxation persist above T(g)? Phys. Rev. Lett. **91**, 115701 (2003)
54. K.L. Ngai, *Relaxation and diffusion in complex systems* (Springer, New York, 2011)
55. K.L. Ngai, An extended coupling model description of the evolution of dynamics with time in supercooled liquids and ionic conductors, J. Phys.: Condens. Matter **15**, S1107 (2003)
56. S. Capaccioli, K.L. Ngai, Relation between the alpha-relaxation and Johari-Goldstein beta-relaxation of a component in binary miscible mixtures of glass-formers, J. Phys. Chem. B **109**, 9727 (2005)